The Journal of Chemical Physics

RESEARCH ARTICLE | APRIL 26 2024

Probing the electronic structure and ground state symmetry of gas phase C_{60}^+ via VUV photoionization and comparison with theory

Helgi Rafn Hrodmarsson ; Mathias Rapacioli ; Fernand Spiegelman ; Gustavo A. Garcia ; Jordy Bouwman ; Laurent Nahon ; Harold Linnartz

J. Chem. Phys. 160, 164314 (2024)
https://doi.org/10.1063/5.0203004

AIP Publishing

The Journal of Chemical Physics ARTICLE pubs.aip.org/aip/jcp

Probing the electronic structure and ground state symmetry of gas phase C_{60}^+ via VUV photoionization and comparison with theory

Cite as: J. Chem. Phys. 160, 164314 (2024); doi: 10.1063/5.0203004
Submitted: 8 February 2024 • Accepted: 8 April 2024 •
Published Online: 26 April 2024

Helgi Rafn Hrodmarsson,[1,a] Mathias Rapacioli,[2] Fernand Spiegelman,[2] Gustavo A. Garcia,[3] Jordy Bouwman,[4,5,6] Laurent Nahon,[3] and Harold Linnartz[1]

AFFILIATIONS

[1] Laboratory for Astrophysics, Leiden Observatory, Leiden University, P.O. Box 9513, NL-2300 RA Leiden, The Netherlands
[2] Laboratoire de Chimie et Physique Quantiques LCPQ/FeRMI, UMR5626, Université de Toulouse (UPS) and CNRS, Toulouse, France
[3] Synchrotron SOLEIL, L'Orme des Merisiers, St. Aubin, BP 48 Gif sur Yvette, France
[4] Laboratory for Atmospheric and Space Physics, University of Colorado, Boulder, Colorado 80303, USA
[5] Department of Chemistry, University of Colorado, Boulder, Colorado 80309, USA
[6] Institute for Modeling Plasma, Atmospheres, and Cosmic Dust (IMPACT), University of Colorado, Boulder, Colorado 80303, USA

[a] **Present address:** LISA UMR 7583 Université Paris-Est Créteil and Université de Paris, Institut Pierre et Simon Laplace, 61 Avenue du Général de Gaulle, 94010 Créteil, France.
Author to whom correspondence should be addressed: hhrodmarsson@lisa.ipsl.fr and hr.hrodmarsson@gmail.com

ABSTRACT

Recently, some of us reviewed and studied the photoionization dynamics of C_{60} that are of great interest to the astrochemical community as four of the diffuse interstellar bands (DIBs) have been assigned to electronic transitions in the C_{60}^+ cation. Our previous analysis of the threshold photoelectron spectrum (TPES) of C_{60} [Hrodmarsson *et al.*, Phys. Chem. Chem. Phys. **22**, 13880–13892 (2020)] appeared to give indication of D_{3d} ground state symmetry, in contrast to theoretical predictions of D_{5d} symmetry. Here, we revisit our original measurements taking account of a previous theoretical spectrum presented in the work of Manini *et al.*, Phys. Rev. Lett. **91**(19), 196402 (2003), obtained within a vibronic model parametrized on density functional theory/local-density approximation electronic structure involving all h_g Jahn–Teller active modes, which couple to the ^2H_u components of the ground state of the C_{60}^+ cation. By reanalyzing our measured TPES of the ground state of the C_{60} Buckminsterfullerene, we find a striking resemblance to the theoretical spectrum calculated in the work of Manini *et al.*, Phys. Rev. Lett. **91**(19), 196402 (2003), and we provide assignments for many of the h_g modes. In order to obtain deeper insights into the temperature effects and possible anharmonicity effects, we provide complementary modeling of the photoelectron spectrum via classical molecular dynamics (MD) involving density functional based tight binding (DFTB) computations of the electronic structure for both C_{60} and C_{60}^+. The validity of the DFTB modeling is first checked vs the IR spectra of both species which are well established from IR spectroscopic studies. To aid the interpretation of our measured TPES and the comparisons to the *ab initio* spectrum we showcase the complementarity of utilizing MD calculations to predict the PES evolution at high temperatures expected in our experiment. The comparison with the theoretical spectrum presented in the work of Manini *et al.*, Phys. Rev. Lett. **91**(19), 196402 (2003), furthermore, provides further evidence for a D_{5d} symmetric ground state of the C_{60}^+ cation in the gas phase, in complement to IR spectroscopy in frozen noble gas matrices. This not only allows us to assign the first adiabatic ionization transition and thus determine the ionization energy of C_{60} with greater accuracy than has been achieved at 7.598 ± 0.005 eV, but we also assign the two lowest excited states ($^2E_{1u}$ and $^2E_{2u}$) which are visible in our TPES. Finally, we discuss the energetics of additional DIBs that could be assigned to C_{60}^+ in the future.

I. INTRODUCTION

The Diffuse Interstellar Bands (DIBs) have remained an elusive mystery since the first bands were detected by Heger over a century ago.[1] Despite our knowledge of molecular complexity in space having been increasing in an accelerated manner in recent years,[2] only one molecule has been assigned as a DIB carrier thus far, namely the C_{60}^+ cation which has four DIBs assigned in the 5780–6615 Å region.[3–5] Recent work extends on this by proposing the C_{60}–Fe^+ complex as a possible carrier[6] but C_{60}^+ has also been found in reflection nebulae through its mid-IR fingerprints.[7] Despite C_{60}^+ claiming the honor of being the first molecule to be unambiguously identified as a DIB carrier, the nature of the electronic transitions behind these DIBs is not fully understood and in part this been because of the debated nature of the equilibrium molecular geometry of C_{60}^+ in its electronic ground state.

As C_{60} belongs to the extremely symmetric icosahedral (I_h) point group, the states resulting from the removal of an electron in the fivefold degenerate highest occupied molecular orbital HOMOs with h_u symmetry are subject to Jahn–Teller (JT) deformation. Actually, two lowest stable energy conformations of C_{60}^+ with respectively D_{5d}, and D_{3d} symmetry have been theoretically predicted,[8–10] the D_{5d} conformation being the lowest one, namely −129 meV with respect to the I_h reference vs −39 meV for the D_{3d} conformation from Density Functional Theory calculations (CAM-B3LYP/DFT) calculations.[11] Beyond this static JT deformation, vibration may induce tunneling between the multi-fold equivalent conformers, leading to pseudo-rotation features[12,13] or dynamical JT effects, while nonadiabatic electron-vibrational coupling is necessary to determine the precise vibronic states. Experimental infrared absorption spectroscopy on C_{60}^+ in frozen noble gas matrices showed that C_{60}^+ better corresponds to D_{5d} symmetry with the assignments of several bands.[8] Recently, assignments of two bright band doublets in the near-IR region at 9428/9577 and 9365/9632 Å to C_{60}^+ have been theoretically proposed from TD-DFT CAM-B3LYP calculations.[14] Computations also predicted that the ground state vibrational motion could extend over the ground state potential surface thus leading to so-called "non-vertical transitions" (away from the D_{5d} conformation) toward C_{60}^+ excited states themselves presenting further symmetry breaking and pseudo-JT energy lowering when departing from D_{5d} symmetry.[14]

Interestingly, the question of the equilibrium molecular geometry of the C_{60}^+ cation in the ground electronic state has also led to some debate[15,16] in the interpretation of the photoelectron spectrum (PES) of C_{60}.[17] The triplet structure observed by Canton *et al.*[17] at 230 and 390 meV above the supposed ground state was interpreted as being the result of vibronic coupling due to a JT dynamical split of a ground cationic state of reduced D_{3d} symmetry. Subsequently, Manini and Tosatti[16] argued that the tunnel splitting should be an order of magnitude smaller than the first two peaks separation in the recorded PES. Manini *et al.*[18] subsequently developed a vibronic model based on Density Functional Theory (DFT) calculations of the potential energy surfaces and provided a fair interpretation of the PES features observed by the authors of the work of Canton *et al.*[17]

Recently, we measured the first threshold photoelectron spectrum (TPES) of C_{60}.[19] The initial inspection of the ground state showed a similar splitting that was described in the work of Canton *et al.*[17] which led to an assignment of the C_{60}^+ ground state as exhibiting D_{3d} symmetry rather than D_{5d}. Here, we revise this interpretation by re-investigating our previous dataset, arriving at better energy resolution that allows JT-active vibrational modes to be resolved. We compare our reanalyzed TPES with the previously simulated photoelectron spectrum presented in the work of Manini *et al.*,[18] based on DFT calculations of the electronic states and couplings and on the resolution of a vibronic model including the five H_u electronic states and 66 vibrational harmonic oscillators.[20] It should be noted that the work of Manini *et al.*[18] was based on reduced dimensionality and harmonic approximations of the basis of vibrational modes and did not include the effects of anharmonicities in the potential surfaces that might possibly contribute to spectral shifts at temperatures such as those encountered in our experiment where C_{60} was sublimated in an oven at 600 °C and seeded in a molecular beam. Also, the model presented in the work of Manini *et al.* did not include the contributions of the a_g and g_g modes. This is discussed in the next sections.

This paper is constructed as follows. In Sec. II we describe the experimental and theoretical methodologies. In Sec. III, we show and discuss our results in the following order. First, we estimate the temperature in the molecular beam in our experiment such that a theoretical PES can be provided for appropriate comparisons with the re-treated experimental TPES. We will show how the calculations compare with our experiment to eventually arrive at an assignment of the adiabatic ionization transition and how the simulated *ab initio* PES presented in the work of Manini *et al.* compares with our re-treated TPES. This comparison gives credence to D_{5d} symmetry for C_{60}^+ in the gas phase and we present tentative assignments to several of the JT-active h_g bands. We also revisit the assignment of our TPES and compare them with the previously calculated PES presented in the work of Manini *et al.*,[18] and with the more recent calculations of the h_g and g_g vibrational modes (uncoupled) and vibronic parameters by Huang and Liu.[11] The new assignment allows us to obtain an ionization energy of C_{60} with greater accuracy than ever before. In order to complement the discussion, we examine the possible role of temperature and anharmonicities for C_{60} and C_{60}^+ on vibrational spectra via density functional based tight binding (DFTB) molecular dynamics simulations at various temperatures. Subsequently, we determine a DFTB-calculated PES via classical molecular dynamics (MD)—non-vibrationally resolved—and estimate the effects of temperature on the simulated photoelectron spectrum. This also helps us shed light on the comparison of our TPES and the recent IR and electronic spectra of C_{60}^+ presented in the work of Kappe *et al.*,[21] which allows us to identify and tentatively assign the $^2E_{1u}$ and $^2E_{2u}$ electronically excited states in our TPES. In Sec. IV, we discuss the DIBs assigned to excitations in the C_{60}^+ cation and whether more potential DIBs may be observed and assigned to C_{60}^+ in the future. The newly assigned 0–0 transition and the energy differences between peaks in the second photoelectron band are in good agreement with previously measured electronic excitations of C_{60}^+.[22–24] We conclude with a summary.

II. METHODOLOGIES

A. Experimental

The experimental details of the measurements of the TPES of C_{60} have been described previously.[19] Hence, only a brief outline will be described here. Experiments were performed on the DESIRS

VUV beamline at the Synchrotron SOLEIL facility,[25] using horizontally polarized radiation in the range 6–10 eV. The photon beam was dispersed by a 6.65 m normal incidence monochromator before it interacted with the molecular beam at a right angle inside the double imaging photoelectron photoion coincidence (i^2PEPICO) spectrometer DELICIOUS III on the permanent endstation SAPHIRS,[26] which connects with DELICIOUS III via a two-stage differential pumping scheme.[27] Inside SAPHIRS, C_{60} was sublimated at 600 °C and Ar was used as a carrier gas with a low backing pressure of 0.2 bars. The recorded electron images at each photon energy were Abel inverted using the pBasex algorithm[28] such that the ionization intensities could be plotted in matrix form as a function of the electron kinetic energy and photon energy.[29] The TPES was constructed by integrating the pixel intensities along the electron signals in the matrix from KE_{max} = 0 to a fairly small value—typically varying from 5 to 75 meV depending on the signal strength. In our previous work, this value was 50 meV, resulting in a total energy resolution of 13 meV, which was based on a convolution of the electron bandwidth used to create the TPES and the photon resolution.[19] The photon energy resolution is estimated between 6.0 and 6.5 meV in the energy region of the first photoelectron band of C_{60}. In this work, we revisit this TPES treatment and present the TPES constructed with 10 and 25 meV as the maximum allowed electron kinetic energy signals. The smaller values used as KE_{max} result in smaller values of the resolution from the electron bandwidth and hence the total energy resolution of the spectrum: 8 meV for KE_{max} = 10 meV, and 11 meV for KE_{max} = 25 meV. The accuracy of the energy scale is slightly better, or 5 meV (half the energy step), as determined through the various ionization energies of background contaminants such as O_2 (12.07 eV), H_2O (12.62 eV) and the residual second harmonic ionization of argon (7.88 eV). We can thus give an overall accuracy of our values as ±5 meV.

B. Theoretical

A series of density functional-based tight binding (DFTB) calculations[30,31] were performed to compute temperature-dependent IR and photoelectron spectra. All DFTB calculations in this work were carried out with the deMonNano code.[32] In its self-consistent charge (SCC) formulation, DFTB is derived from DFT through a second order expansion of the DFT energy around a reference density, taken as the sum of the individual isolated atomic densities. The neglect of the three-center integrals allows building the DFTB Kohn Sham operator from two-center pre-tabulated DFT data and the second order contribution is computed from atomic charges (computed within the Mulliken scheme) and Hubbard-like atomic parameters. In this work, we have used the matsci parameters.[33] Considering these approximations, DFTB is computationally very efficient and can be incorporated in extensive MD simulations with all nuclear degrees of freedom at various temperatures.

The harmonic IR spectra of both C_{60} and C_{60}^+ were computed through diagonalization of the weighted Hessian matrices, which gave the frequencies of the normal modes. The temperature-dependent IR spectra were computed from molecular dynamics trajectories as detailed previously.[34] For a given desired temperature, the system was first thermalized by means of molecular dynamics (MD) simulations of 50 ps (time step of 0.5 fs) in the canonical ensemble using a Nose–Hoover chain of 5 thermostats at a frequency of 800 cm^{-1}. A total of 31 snapshots (geometries and velocities) equally spaced along this trajectory are used to generate initial conditions for further MD simulations performed in the microcanonical ensemble. Each one of these NVE simulations lasts 25 ps and a spectrum is produced from the Fourier transform of the autocorrelation molecular dipole moment. The 31 spectra were averaged to produce the spectrum at the desired temperature. The full process has been reproduced for 9 temperatures ranging from 50 to 1500 K as an appropriate sample size to explore the effects at various temperatures. As detailed below, at the highest temperatures the spectral signatures of the specific modes become hardly discernible. A weighted factor of 0.92 was applied to all the DFTB computed frequencies but this scaling value was determined to provide better agreement with prior work, in particular with the higher frequencies.

To simulate the temperature-dependent photoelectron spectra, we used DFTB to generate neutral C_{60} configurations from parallel-tempering molecular dynamics simulations and the ground state of C_{60}^+ and TD-DFTB to access the excited states spanned by holes created in the five highest occupied orbitals of C_{60}^+. In the D_{5d} equilibrium geometry, the fivefold degenerate ^2H_u state splits into $^2A_{1u}$ (nondegenerate) and $^2E_{1u}$ and $^2E_{2u}$ (doubly degenerate) components. In MD, the degeneracy is essentially fully lifted. In this scheme, 60 MD simulations with temperatures ranging from 50 to 1300 K (same thermostat as reported above but larger time step of 0.75 fs to favor a more complete exploration at fixed computational time) were performed in parallel and exchanges between the different replicas are periodically attempted to increase ergodicity.[35,36] For each temperature, 2700 structures were extracted and, for each of them, we computed the energies of both the neutral and cationic ground states as well as the energies of the excited electronic states of the cation from a time-dependent DFTB calculation.[37,38] The photoelectron spectrum was then built by accumulating in a single histogram with a bin size of 2 meV, for each one of the 2700 structures, all the possible vertical (Franck–Condon) transitions from the neutral ground state to the cationic ground state. This included contributions from the five excited states created by each of the holes in the five highest orbitals of C_{60}^+. We note that, as we have no access to the transition dipole intensity from the neutral ground state to any electronic states of the cation (ground state or excited state), we attribute the same intensity (value of 1 in practice) to all possible ionization transitions. Moreover, vibration is treated classically, so that while the dynamical Jahn–Teller effect is accessible, quantum vibrational resolution within the simulation is out of reach.

III. RESULTS AND DISCUSSION

A. Molecular beam temperature

One of the main questions or uncertainties concerning the previously obtained TPES of C_{60} concerns the precise temperature of the contents in the molecular beam expansion as the temperature profile would allow us to apply an appropriate finite temperature to estimate the anharmonicity of the JT-active modes in the *ab initio* PES presented in the work of Manini *et al.* This would allow us to better decipher the 0–0 transition and which features of the TPES belong to hot bands (see below).

Although the oven from which C_{60} was vaporized was kept at 600 °C (873 K) during experiments, this temperature does not

directly translate to an internal and/or translational temperature profile of the molecular beam. There are ways to determine the temperature of the embedded C_{60} molecules though. One way is to extract a translational temperature of the C_{60} molecules by inspecting the velocities of the components of the molecular beam, namely Ar (the carrier gas) and C_{60}, when they are projected along the direction of the molecular beam.

In molecular beams, the temperature ratio (T/T_0) depends on the Mach number and on the heat capacity ratio of the gas (γ), where T_0 is the nozzle temperature (893 K) and T is the temperature in the molecular beam,

$$\frac{T}{T_0} = \frac{1}{\left(1 + \frac{\gamma-1}{2} * M^2\right)}.$$

The Mach number itself is defined as

$$M = \frac{v_{jet}}{\sqrt{\frac{\gamma RT}{W}}},$$

where W is the mass, v_{jet} is the jet velocity, R is the ideal gas constant, T is the temperature, and γ is the specific heat ratio. For Ar and C_{60}, the velocities all peak at the same value, around 870 m/s (see Fig. S1 in the supplementary material), as expected. At 870 m/s, the temperature of the molecular beam can be estimated at 145 K considering a pure Ar beam.

Another way to estimate the translational temperature is from the widths of the velocity distributions since $T = \frac{FWHM^2 M}{8R \ln(2)}$, where M is the molar mass. For Ar and C_{60}, this gives 120 and 735 K, respectively. The values obtained from the two approaches are pretty similar where the slight difference in the temperature of Ar could be explained by a few % concentration of C_{60}. This leads us to assume that the temperature of C_{60} extracted from the width of its velocity component along the molecular beam is a decent estimate of the translational temperature of C_{60}. The disparity between the temperatures of the carrier gas vs C_{60} may not be surprising as for translational cooling to be the most efficient, carrier gases should be of comparable mass to the molecules embedded.

The temperature estimated for C_{60} in the molecular beam (735 K) will lead to temperature-induced spectral shifts that are dependent on the ω_0 mode in question. Hence, the larger the energy needed to excite a vibrational mode, the larger the expected shift. For example, for the combination band around 1600 cm^{-1}, a shift of 35 cm^{-1} (4.4 meV) is expected at 735 K for an anharmonicity parameter of $p = -3 \times 10^{-5}$ K^{-1} (see below). If we allow for a 200 K uncertainty on the temperature, then its upper limit could be extended to roughly a 6 meV red shift of the largest JT-active modes.

Of course, we assume here that the system is equilibrated, i.e., that the translational, vibrational, rotational temperatures are equivalent, which is an oversimplification. However, as we have a molecular beam that we estimate has almost negligible cooling effects on its C_{60} contents as we were using a large (500 μm) nozzle and very low backing pressure (0.2 bars) for the expansion, we can estimate that the system is close to Boltzmann equilibrium, rather than a cold molecular beam.

B. Comparison between TPES and vibronic PES

Two TPES of C_{60} that were constructed for the purposes of this work are showcased in Fig. 1. The two TPES are obtained by integrating the 2D-PES matrix from KE_{min} = 0 up to either KE_{max} = 10 or 25 meV. For brevity, these two TPES will be referred to as $TPES_{10}$ and $TPES_{25}$, respectively.

The top panels of Fig. 1 compare the two TPES (black) with the theoretical PES results (blue) presented in the work of Manini *et al.* at T = 0 K.[18] $TPES_{10}$ (top left panel) shows a remarkable agreement with the theoretical curve between 7.60 and 7.75 eV, but above that energy, the calculated peaks align a bit worse with the experimental ones. A possible cause for the offset could be the harmonic oscillator approximation in the vibronic model and the neglect of anharmonicities in the potential energies and/or couplings, the use of the local density approximation (LDA) functional in the determination of vibronic coupling or possible coupling to other modes. Meanwhile, if we accept the validity of this comparison around the ionization onset, we can assign the 0–0 transition and measure the adiabatic ionization energy as 7.598 ± 0.005 eV. $TPES_{25}$ (top right panel) shows better agreement for the latter half of the spectrum and a slightly worse agreement with the first half of the spectrum where there appear to be some broadenings after the ionization onset (i.e., between 7.6 and 7.8 eV).

The authors of the work of Manini *et al.* also determined an *ab initio* spectrum computed at 300 K. In the middle panels of Fig. 1, this spectrum is compared to our $TPES_{10}$ and $TPES_{25}$. Again, the comparison for the first few bands is practically perfect and even more impressive is how well the positions of the hot bands in the computed spectrum match the experiment. For both $TPES_{10}$ and $TPES_{25}$, the shape of the latter half of the spectrum aligns well with the general continuum observed in the experiment. However, the experimental spectra display multiple further features, which do not fully match the theoretical ones, and are manifested as spectral shifts and unidentified or unresolved peaks. A zoomed-in view of the TPES in the range 7.76–7.90 eV is given in Fig. S2. The $TPES_{10}$ data appear to match well with the peaks in the theoretical spectrum apart from the peak around 7.85 eV that appears to be missing. However, the latter peak is present in $TPES_{25}$ but the peaks predicted by the theoretical spectrum at 7.811, 7.831, and 7.852 eV appear shifted to the blue (by 3–11 meV) with respect to the experimental peaks observed at 7.808, 7.825, and 7.851 eV.

It appears that the $TPES_{10}$ signal in Fig. S2 is too weak for the 7.85 eV *ab initio*-predicted peak to be visible. However, by increasing the electron bandwidth (and thus increasing the signal at the cost of energy resolution), all the peaks predicted in the theoretical spectrum become visible but appear shifted by between ~3 and 11 meV. Below, we will discuss how sound the agreements are between the theoretical spectrum and both $TPES_{10}$ (particularly for the first several bands and hot bands) and $TPES_{25}$ with respect to anharmonicities below.

The best fit of the FC envelope calculated in the work of Manini *et al.* to our data is obtained for an adiabatic ionization energy of 7.598 ± 0.005 eV. Although the experimental signal-to-noise ratio is not sufficient for a complete match of all possible vibronic transitions, some of the predicted features are present in the experimental spectrum, especially in the region 7.5–7.8 eV where the S/N is

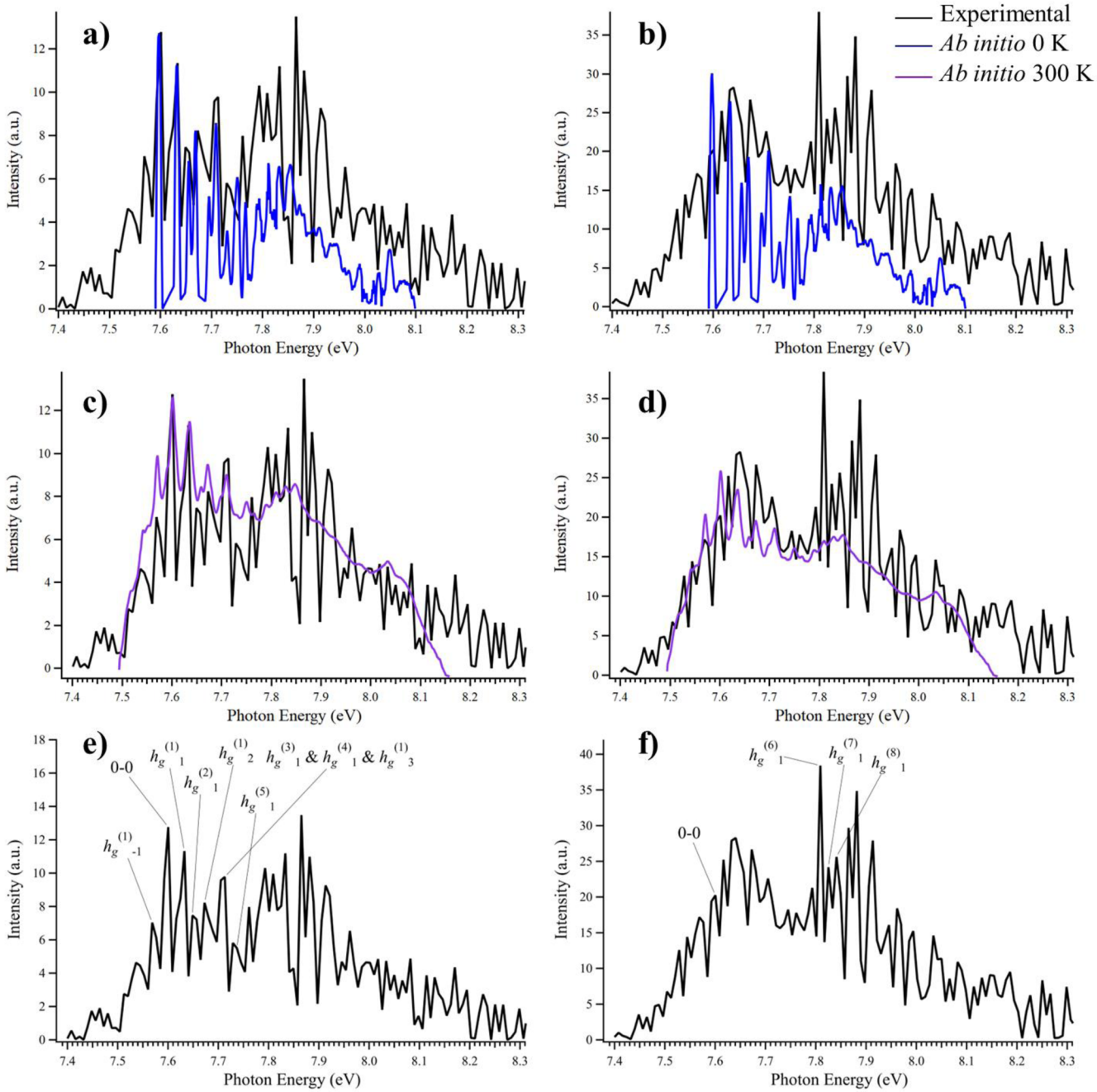

FIG. 1. Comparison of experimental TPES (black traces) and *ab initio*-based PES from Ref. 18. Panels (a) and (c) portray the KE_{max} = 10 meV TPES and panels (b) and (d) the KE_{max} = 25 meV. A*b initio*-computed PES at 0 K (blue traces—top) and 300 K (purple traces—middle). Panels (e) and (f) show assignments of h_g modes in $TPES_{10}$ and $TPES_{25}$.

acceptable, as shown in the comparisons in Table I. This allows us to make some assignments through the comparison with the theoretical spectrum, the most important of which is the 0–0 transition along with the first few h_g modes as well as convolutions with some of their overtones [see Figs. 1(e) and 1(f)]. These assignments are essentially based on the assignments made in the work of Manini *et al.*[18] Despite the limitations of the vibronic model (based on DFT/LDA calculations and relying on the harmonic oscillator representation), the

TABLE I. Comparison of the observed peaks in our measured $TPES_{10}$ and $TPES_{25}$ with the frequencies of the vibronic model calculated by Manini *et al.* (LDA) and Huang and Liu (B3LYP, CAMB3LYP) and the harmonic frequencies of C_{60} (I_h) and C_{60}^+ (D_{5d}) obtained with DFTB (this work). For DFTB levels, a corrective multiplicative factor 0.92 was applied (see text) and the relevant harmonic frequencies are given within parentheses.

$TPES_{10}$ peaks (meV/cm^{-1})	$TPES_{25}$ peaks (meV/cm^{-1})	DFT frequencies (cm^{-1}) LDA/B3LYP/ CAM-B3LYP	Symmetry (I_h)	DFTB harmonic C_{60}	Symmetry (D_{5d})	DFTB harmonic C_{60}^+
32/258	36/290	261/266/271	$h_g^{(1)}$	250 (272)	e_{1g},e_{2g},a_{1g}	227,234,250 (247,255,271)
52/419	56/451	429/439/450	$h_g^{(2)}$	405 (438)	e_{2g},e_{1g},a_{1g}	401,402 (412,436,437)
		483/481/502	$g_g^{(1)}$	466 (506)	e_{1g},e_{2g}	445,456 (484,496)
		500/497/506	$a_g^{(1)}$	509 (553)	a_{1g}	509(553)
		567/584/586	$g_g^{(2)}$	555 (603)	e_{2g},e_{1g}	554,555 (602,603)
72/581		718/726/745	$h_g^{(3)}$	656 (713)	a_{1g},e_{1g},e_{2g}	655,684,687 (712,744,747)
		772/768/787	$g_g^{(3)}$	689 (749)	e_{1g},e_{2g}	710,715 (772,778)
108/971		785/786/802	$h_g^{(4)}$	794 (864)	e_{1g},e_{2g},a_{1g}	783,786,790 (851,854,859)
		1111/1092/1092	$g_g^{(4)}$	1105 (1202)	e_{1g},e_{2g}	1013,1034 (1101,1124)
132/1065	136/1096	1119/1125/1148	$h_g^{(5)}$	1138 (1238)	e_{2g},e_{1g},a_{1g}	1135,1140,1141 (1234,1240,1241)
161/1299	161/1299	1275/1269/1300	$h_g^{(6)}$	1299 (1413)	e_{2g},a_{1g},e_{1g}	1238,1284,1301 (1346,1396,1414)
		1322/1335/1356	$g_g^{(5)}$	1334 (1450)	e_{1g},e_{2g}	1328,1329 (1443,1445)
193/1556	193/1556	1456/1443/1480	$h_g^{(7)}$	1470 (1598)	e_{2g},a_{1g},e_{1g}	1457,1475,1477 (1584,1603,1605)
		1511/1498/1527	$a_g^{(2)}$	1506 (1637)	a_{1g}	1512 (1644)
		1519/1540/1576	$g_g^{(6)}$	1538 (1696)	e_{1g},e_{2g}	1512,1551 (1644,1686)
209/1686	209/1686	1588/1607/1663	$h_g^{(8)}$	1615 (1779)	e_{2g},e_{1g},a_{1g}	1590,1632,1639 (1729,1775,1782)

comparisons between the $TPES_{10}$/$TPES_{25}$ and the theoretical spectrum are impressive, although the model does not account for the g_g and a_g modes expected from the H ⊗ (a + g + h) JT model.[12,39] The offsets mentioned above could be due to the neglect of off-diagonal anharmonicities in the potential energies and/or couplings, the use of the LDA functional in the determination of the vibronic coupling or possible coupling to other modes. Recently, Huang and Liu[11] reparametrized a vibronic model employing better functionals: B3LYP and CAM-B3LYP. The frequencies of their basis of harmonic oscillators occurred to be quite close to the parametrization used in the work of Manini *et al.* while the electron–vibration couplings seem different. Unfortunately, Huang and Liu.[11] only investigated the static Jahn–Teller effects and did not determine the vibronic levels. For this reason, we have chosen to assign in Table I our experimental TPES peaks following the h_g levels only, as provided in the work of Manini *et al.*[18] Note that the coupled vibronic levels calculated by Manini are generally quite close to the frequencies of the uncoupled oscillators. We are confident in the assignments of the two lower $TPES_{10}$ peaks at 258 and 419 cm^{-1} to the $h_g^{(1)}$ and $h_g^{(2)}$ theoretical modes, respectively. Moreover, the $TPES_{25}$ peaks from 1096 to 1686 cm^{-1} can be assigned to the $h_g^{(5)}$–$h_g^{(8)}$ modes. It is evident that some peaks present in the experimental TPES, such as $h_g^{(3)}$ and $h_g^{(4)}$, do not line up as well with the data presented in the work of Manini *et al.* The positions of the experimental peaks at 581 and 1096 cm^{-1} closely match the positions of the $g_g^{(2)}$ and $g_g^{(5)}$ modes, but these might be coincidental. The authors of the work of Manini *et al.* did not include the a_g and g_g modes in their computed spectrum as their previous work[20] showed that in D_{5d} symmetry, the $a_g^{(1)}$ and all the g_g modes did not contribute to the stabilization energy of cation. However, the more recent work by Huang and Liu[11] tabulated nonzero stabilization energies for the $g_g^{(3)}$ and $g_g^{(4)}$ modes that are on par with those of the $h_g^{(2)}$ and $h_g^{(4)}$ modes. Hence, the $h_g^{(3)}$ and $h_g^{(4)}$ assignments should be considered as tentative.

Our TPES can also be compared with the previous IR spectrum of the C_{60}^+-He complex recorded in the work of Gerlich *et al.*[40] and the recently measured electronic spectrum presented in the work of Kappe *et al.*[21] These are compared with $TPES_{10}$ and $TPES_{25}$ in Fig. S3 in the supplementary material where these have been shifted by the ionization energy to compare directly with the TPES. The IR spectrum presented in the work of Gerlich *et al.* has much greater resolution than the TPES, so direct comparisons between the two are moot. However, the electronic spectrum contains structures that appear right around where two intense peaks appear in our TPES: 7.865 and 7.882 eV. Kappe *et al.*[21] also performed TD-DFT calculations, similar to those performed previously by Lykhin *et al.*,[14] on the C_{60}^+ cation, which predicted two dark electronically excited states (i.e., with zero oscillator strengths), $^2E_{1u}$ and $^2E_{2u}$, whose appearance in their spectrum was justified by possible vibronic couplings with the JT-active vibrations of the ground state. The peaks also coincide with an autoionizing resonance, which is evidenced both in the total ion yield recorded previously[41] and the two-dimensional photoelectron spectrum matrix recorded in our previous work.[19] This lends further support for these peaks originating from a different electronic state than the ground state as autoionization resonances producing slow photoelectrons appear when a superexcited state

of the neutral molecule and an electronic state of the ion are very close in energy. There are also a number of peaks resembling vibrational structure to the blue of the two intense peaks at 7.865 and 7.882 eV, and while there are some correspondences between our TPES and the electronic spectrum measured in the work of Kappe *et al.*[21] in Fig. S3, assigning these is out of the current scope of this paper. However, we can nonetheless tentatively assign the two peaks at 7.865 ± 0.005 and 7.882 ± 0.005 eV in our TPES to the $^2E_{1u}$ and $^2E_{2u}$ excited states. This compares very well with the calculated predictions made in the work of Kappe *et al.*[21] who calculated the $^2E_{1u}$ state at 2140 cm^{-1} (or 0.265 eV) above the ground state, which corresponds to 7.862 eV in our TPES, and the $^2E_{2u}$ state at 2190 cm^{-1} (0.271 eV) above the ground state, which corresponds to 7.870 eV in our TPES.

C. Anharmonicities in IR spectra with MD-DFTB

Anharmonic effects are likely to be present both in the initial state, namely vibrational states of C_{60}, and those of the final state C_{60}^+. For neutral C_{60} molecules whose ground state icosahedral symmetry has not been broken, only four t_{1u} out of 46 symmetry unique modes are IR-active.[42] In solid C_{60}, weak resonances have also been observed that have been attributed to anharmonic couplings and/or symmetry reduction from the environment.[43] These IR-active modes are sensitive to temperature as it was shown that their positions shift toward lower energies with increasing temperature; e.g., the $t_{1u}(4)$ mode is red-shifted by 40 cm^{-1} at a temperature of 1830 K as compared to its value at 875 K. Computed IR spectra of neutral C_{60} are shown in Fig. 2. Assignments can be found in the work of Nemes *et al.* who derived their mode numberings from solid state works[44,45] and previous theoretical work where IR- and Raman-active modes were all calculated for C_{60}.[46–49]

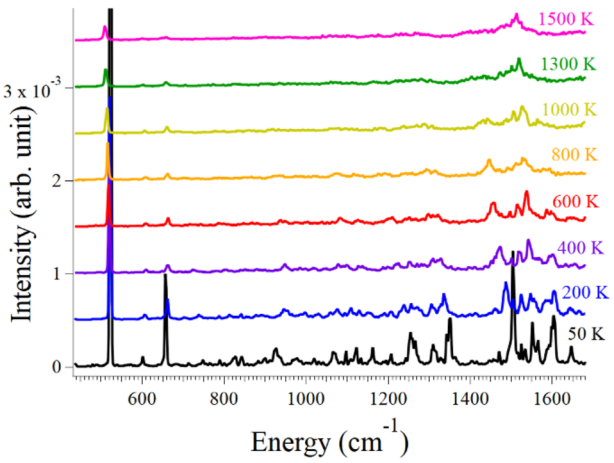

FIG. 2. DFTB-computed IR spectra of C_{60} at temperatures ranging from 50 to 1500 K in the 400–1800 cm^{-1} energy range. The spectra are color-coded as each temperature shown on the right side of the figure.

Previous measurements of the IR spectrum of C_{60} found the four active t_{1u} bands at 518, 557, 1145, and 1397 cm^{-1} in addition to a band at 1525 cm^{-1}.[43] Here, the DFTB computed harmonic frequencies scaled by the aforementioned 0.92 factor are calculated at 483, 596, 1227, and 1446 cm^{-1} which is consistent with the low temperature MD simulation. However, it also shows other small peaks resulting from vibrational symmetry breaking. This temperature evolution of the peaks is in line with previously observed trends.[50] The peaks shift to the red and show substantial broadening resulting from vibrational departure from symmetry, anharmonicities, as well as partially merging at higher temperatures. From these simulations given in Fig. 2, one can derive an anharmonicity parameter[51] $p = \frac{1}{\omega_0}\frac{d\omega}{dT}$ with ω_0 as the vibrational frequency at T = 0 K. Our results give p between -1.8×10^{-5} and -4.0×10^{-5} K^{-1}, which compares well with prior calculations,[51] which used a moment method and a Tersoff potential for C_{60}, leading to anharmonicities between -2×10^{-5} and -4×10^{-5} K^{-1}. Experimental results are available in the work of Bekkerman *et al.*,[50] who measured thermally induced red shifts of the IR absorption of very hot C_{60} molecules. Using their theoretical values at 0 K and comparing them with their experimental values obtained at 1870 K, we obtain anharmonicities between -1.8×10^{-5} and -2.9×10^{-5} K^{-1}. Other measurements presented in the work of Nemes *et al.*[43] found anharmonicities of the order -0.6×10^{-5} to -1.8×10^{-5} K^{-1}, whereas measured IR spectra of solid C_{60} films have yielded values from -0.8×10^{-5} to -2×10^{-5} K^{-1},[52] and C_{60} embedded in KBr pellets yielded values between -0.8×10^{-5} and -2×10^{-5} K^{-1} up to 523 K.[53] Thus, the DFTB results are consistent with experimental magnitudes of the anharmonicities for C_{60}. Assuming a maximum temperature of 735 K in the present experiment, an upper limit for the shifts can be estimated around 3.0 meV, which is too small to support the largest shifts as documented in Fig. S2 in the supplementary material.

Concerning the cation C_{60}^+ IR spectroscopy, only a few experimental IR direct absorption spectra are available in the literature. Some have been recorded in cryogenic matrices[8,54] but helium messenger spectroscopic technique has also been used to record IR and electronic spectra of C_{60}^+ and its clusters with He.[21,40] In agreement with previous theoretical results, in the matrix studies, the optimized DFTB ground state conformation of C_{60}^+ was found to have D_{5d} symmetry. To check the appropriateness of the DFTB calculations in estimating the magnitude of temperature effects, in the case of C_{60}^+ around a conical intersection, we report in Fig. 3 a series of IR spectra at temperatures ranging from 50 to 1500 K for C_{60}^+. At low temperature, T = 20 K, the C_{60}^+ dynamics explore low energy configurations around the bottom of the Jahn–Teller deformed D_{5d} equilibrium geometry of C_{60}, below the location of the I_h conical intersection. The spectrum is quite rich and shows bands at 380, 410, 530, 650, 800, 1100, 1400, 1450, 1600, 1620, and 1700 cm^{-1} with strong intensities at 530 and 1100 and above 1400 cm^{-1}, in full concordance with the DFTB harmonic frequencies derived from diagonalizing the Hessian matrix. They are also in satisfactory agreement with previous calculations and experimental data presented in the work of Strelnikov *et al.*[54] (with applying the aforementioned 0.92 correction factor). When the temperature is increased, anharmonicities may play an increasing role, however, they show very different regimes below and above temperatures at which

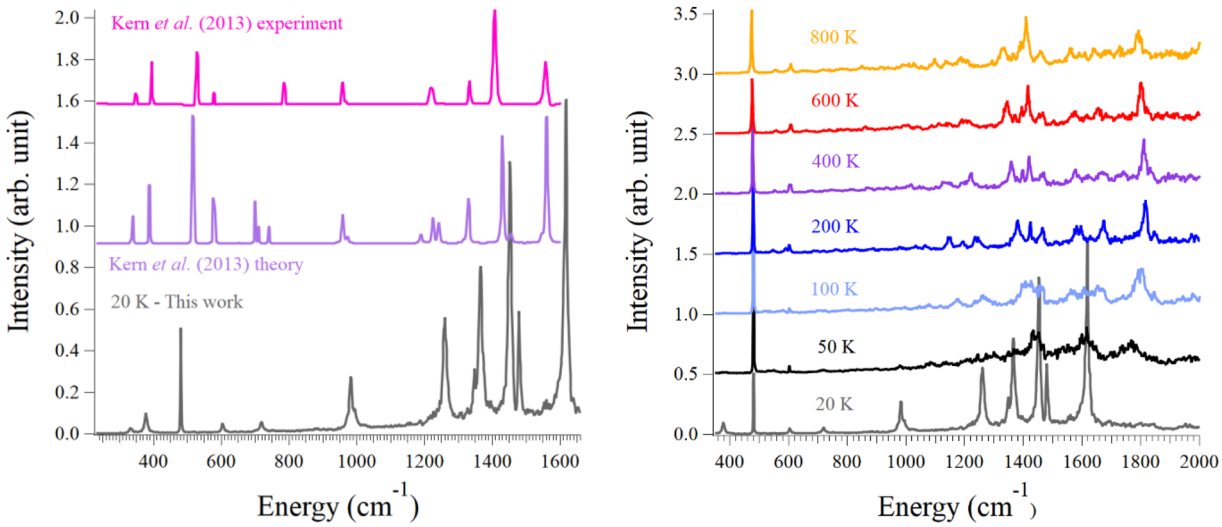

FIG. 3. Comparison and temperature evolution of the IR spectra of C_{60}^+. Left: comparison of the DFTB T = 20 K DFTB-simulated spectrum (corrected by a 0.92 scaling factor, see text) with the absorption experiments at a temperature of 5 K and DFTB/B3LYP-D3 calculations presented in the work of Kern *et al.*[8] Right: MD/DFTB simulation of the temperature evolution in the range 20–1500 K (with the same 0.92 scaling factor).

the conical intersection is currently explored within the MD paradigm. This gives rise to difficulties due to the singularity of the Born–Oppenheimer surface at the conical intersection, which prevents simple fitting as done above in the case of neutral C_{60}, and indeed, the spectrum undergoes significant changes when increasing the temperature from 20 up to 400 K. Only the peak at 530 cm^{-1} remains stable, whereas many of the peaks are smeared out or strongly shifted and broadened. At T = 400 K, the spectral peaks are located at 1250, 1350, 1460, 1500, 1530, 1710, 1820 cm^{-1} and a new peak appears at 1950 cm^{-1}. Thus, it is not possible to presume linear anharmonicity for temperatures below 400 K, while the shifts and widths evolve more regularly for temperatures above 400 K, at which the MD trajectories mostly explore higher energy areas of the potential surface and the details of the JT deformations become less stringent.

D. DFTB-calculated photoelectron spectra of C_{60}

Previously, theoretical attempts have been made to simulate the photoelectron spectra of C_{60} by using a linear coupling scheme that entirely ignores JT effects.[55] While those results compared reasonably with the low-resolution data available at that time, these results do not compare at all with the high-resolution $TPES_{10}$ and $TPES_{25}$ presented above.

At the DFTB level, the adiabatic ionization potential is calculated as 7.567 eV including the harmonic zero-point energy (ZPE) correction difference ΔE_0 = 0.106 eV between the neutral and the ion (7.673 without ZPE), which is in excellent agreement with the experimental value 7.598 eV. Here, it is worth noting that the ZPE, i.e., the lowest harmonic vibration of C_{60}, also corresponds to a kinetic temperature around 700 K in the paradigm described in Sec. II B. Thus, it is useful to define T^* as the temperature designated in the molecular dynamical simulations for a classical system and T as the real temperature of the equivalent quantum system. The C_{60} motion is treated via classical MD in the simulations and therefore does not represent vibrationally resolved features but defining the "classical temperature." T^* is nonetheless useful to explore the conformational space. This introduces a hefty uncertainty in assigning the correspondence between the temperature of the simulations and the experimental one. Hence, we have shifted the temperatures assigned to the simulations by $\Delta\mathbf{T} = 2E_0/k_B(3n - 6)$, where n is the total number of vibrational degrees of freedom of C_{60}, and k_B the Boltzmann constant. Thus, the T^* = 700 K simulation corresponds to the T = 0 K for the quantum system, and T^* = 1000 K simulates a quantum system at temperature of 300 K.

Here, we simulated photoelectron spectra (PESs) using the DFTB methodology outlined in Sec. II B. PESs were calculated at 60 different temperatures ranging from T^* = 50 to 1300 K. In Fig. 4(a), we present the DFTB simulation of the PES (red and black traces). At T = 8 K, it essentially presents two broad features located around 7.6 and 7.75 eV. These broad features are due to the five electronic states resulting from the removal of an electron from each one of the 5 HOMOs [degenerate at the I_h symmetry—Fig. 4(b)], the contributions of which to the full PES are also shown in the figure as sub-components. As already mentioned above, these DFTB/MD simulations cannot display a vibrationally resolved structure. However, the two maxima are in reasonable agreement with the T = 0 K envelope of the vibronic spectra. When the temperature increases, each sub-component gets broadened and the lowest energy peak is slightly red shifted, while the highest energy one is slightly blue shifted. This results in a modal broadening of the DFTB-simulated PES. This is consistent with the effects of temperature visible in the T = 300 K spectra presented in the work of Manini *et al.* This broadening also seems compatible with $TPES_{10}$ and $TPES_{25}$. It is therefore interesting to note that the overall shape of our experimental spectra around the ground cationic state can be explained

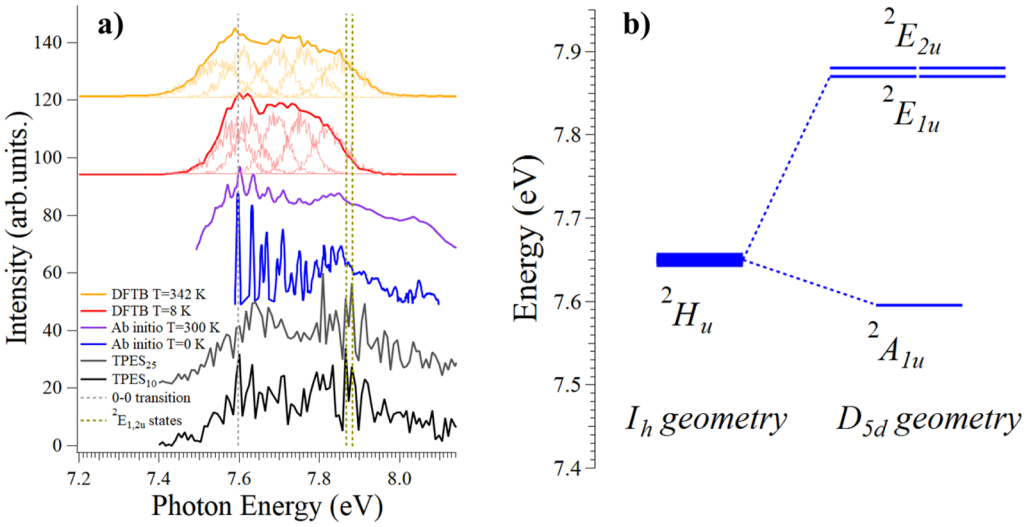

FIG. 4. (a) Comparison of theoretical and experimental TPES. In the DFTB-MD, the "quantum" temperature between parentheses is given by subtracting the ZPE contributions from the classical kinetic energies. In the DFTB-computed spectra, the individual contributions from the five components that are degenerate in I_h geometry are shown underneath each spectrum in a lighter orange and red colors for temperatures T = 342 K and T = 8 K, respectively, and the width of each of the five components is given by the IE of the Boltzmann distribution of the 2700 structures considered. The spectra presented in the work of Manini *et al.*[18] are shown in violet and blue. (b) Energy diagram exhibiting the five-times degenerate ground state of C_{60} at the measured ionization energy and how the degeneracy is lifted upon ionization. Above the ground state, the onsets of the $^2E_{1u}$ and $^2E_{2u}$ electronically excited states are shown.

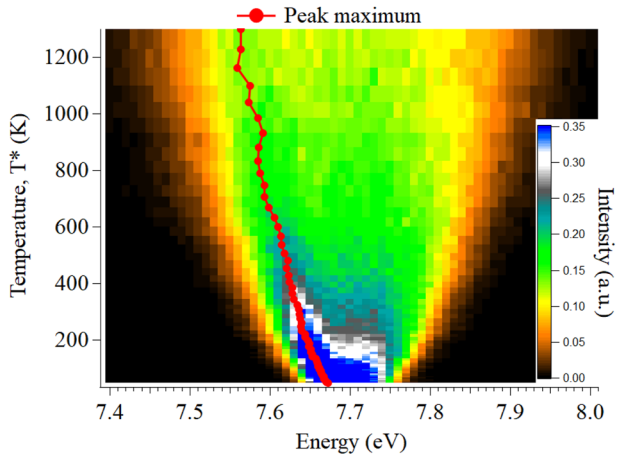

FIG. 5. Heat map of the intensities in the DFTB-calculated PES from 50 up to 1300 K. The red trace indicates the evolution of the lowest energy peak maximum.

through both vibronic transitions within a single conformer whose relative intensities are modeled by the Franck–Condon principle and MD simulations where the broadening stems from the distribution of the five H_u vertical ionization energies within a large conformational population.

Figure 5 summarizes the heat map of the calculated intensities of the DFTB 7.6 eV peak in the classical temperature range 50–1300 K, showing the evolution of the red shift.

IV. ASTROPHYSICAL IMPLICATIONS

With the agreement found with theory, we can give a more in-depth interpretation of the TPES of C_{60} than has been possible before. The *ab initio*-based vibronic model determination of the PES presented in the work of Manini *et al.* allows us to definitively assign the 0–0 transition, which gives us a hereto unprecedented accuracy in the determination of the ionization energy of C_{60}, namely 7.598 ± 0.005 eV. The high resolution of the present experimental work, allowing for vibrational resolution, concludes the question of the interpretation of PES experiments with respect to the symmetry of C_{60}^+ in the gas phase: It provides now a complementary experimental evidence to the IR direct absorption experiments that the ground state of gaseous C_{60}^+ has D_{5d} symmetry rather than D_{3d} symmetry, which previous gas phase photoelectron spectra have alluded to.[17,19]

In an astrophysical context, the assignment of the 0–0 transition allows direct comparison of the recorded TPES of the first electronically excited state (or second photoelectron band) with the energetics of the DIBs that have now already been assigned to transitions in the C_{60}^+ cation. It is worth noting that atoms and molecules in space, and particularly the diffuse interstellar medium, only interact with photons once every few weeks, months, even years. Hence, assigning the 0–0 transition and spectrally locating the absolute ground state of the cation is needed so the energy differences between the 0–0 transition and the structures in the second photoelectron band can be compared to the energetics of the previously assigned DIBs.

Figure 6 superimposes the transitions assigned to the C_{60}^+ DIBs[3–5,56–58] over the TPES starting at the newly assigned

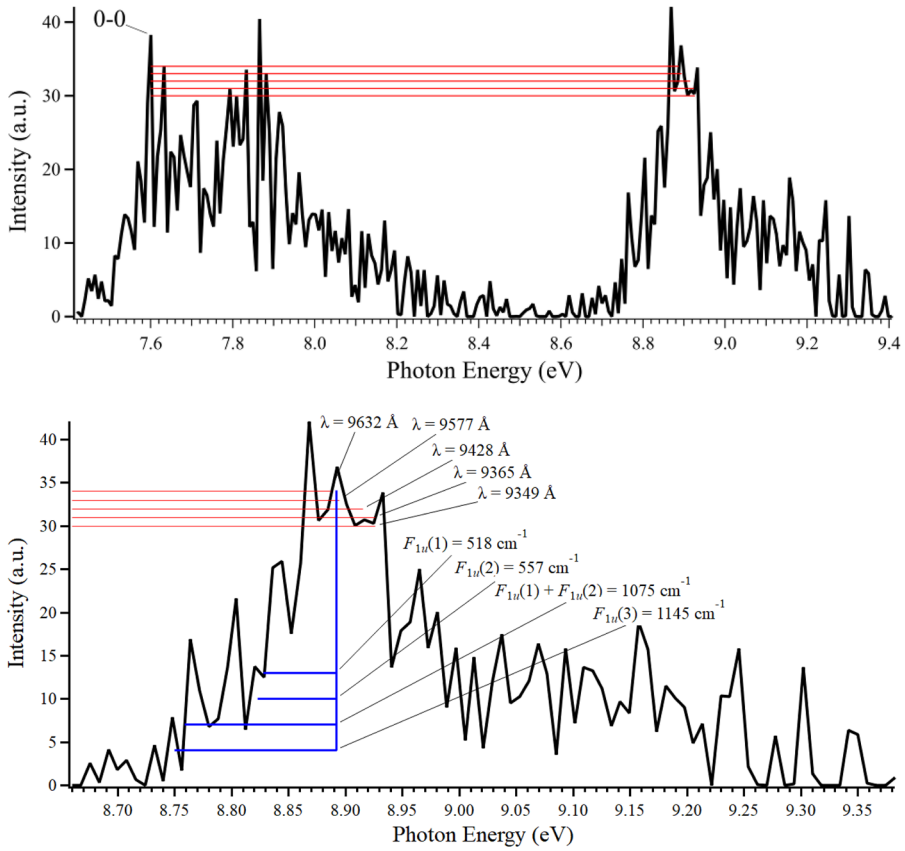

FIG. 6. Top panel: The first two electronic bands of C_{60} in the re-treated $TPES_{10}$. The 0–0 transition is labeled with red lines superimposed on the spectrum. These correspond to the five DIBs that have been assigned to C_{60}^+. Bottom panel: A zoom-in on the second photoelectron band. The apparent locations of the DIBs whose energy levels have been assigned as DIB carriers, assuming our 0–0 assignment in the C_{60}^+ ground state, are shown in red. The blue trace displays the energy displacement expected from vibrations in C_{60} at 875 K. Values are obtained from the study of von Helden *et al.*[59]

0–0 transition. The assigned DIBs correlate well with the energy gap between the 0–0 transition and the peak intensities of the second photoelectron band. Recent theoretical work suggests that the excited state of the C_{60}^+ cation originating with holes in the sub-HOMO orbitals may split from a pseudo-JT effect into C_{2h} symmetry, which includes two vibrational components: A_g and B_g.[14] Unfortunately, the resolution of $TPES_{10}$ is not sufficient to resolve the individual vibronic energy levels of the first excited state in the cation. However, the DIBs appear to correlate well with some of the more intense parts (from 8.893 to 8.933 eV) of the second photoelectron band, but the most intense peak (at 8.869 eV) falls below the lowest DIB. Assuming our 0–0 assignment is correct, this peak would correspond to a hot band. If true, then several hot bands are in fact visible in the TPES, where peaks at 8.764 and 8.804 eV are also observed.

The blue traces in the bottom panel of Fig. 6 show the displacement in energy that are expected from vibrations in C_{60} assuming a high temperature of 875 K (taken from the study of von Helden *et al.*[59] and not far off our assumed experimental temperature of 735 K). While the blue traces do not precisely correspond to peaks, these are still worth mentioning as there are three fundamental modes in C_{60} that could be excited that would contribute to these hot bands on top of a convolution of the first two vibrations. The regular spacing between the peaks ~40 meV apart is similar to the distance between the apparent averages of the $A_g(v' = 0)$ and $B_g(v' = 1)$ states assuming a pseudo-JT effect in the excited state.[14] It would be worth improving on the resolution of this experiment by lowering the temperature of C_{60} embedded in the molecular beam, e.g., with a heavier carrier gas, on top of smaller energy steps and higher signal-to-noise ratio.

What we can say, however, is that between 8.941 and 8.989 eV there is some structure in the TPES that could be due to an agglomeration of higher vibrational modes of the A_g and B_g states. Using our newly obtained value of the ionization energy of C_{60}, these would correspond to peaks between 1.344 and 1.392 eV (i.e., between 8907 and 9225 Å). It is not clear how many peaks one might expect in this range but considering the discrete peaks at 8.965 and 8.981 eV, we could expect some vibrational structure around these energies. In terms of DIBs, these energies, and the uncertainty of the ionization energy (0.005 eV), allow us to predict weak DIBs that could

be assigned to C_{60}^+ around 9063 ± 20 and 8958 ± 20 Å. A wealth of absorption lines exist in these respective energy ranges[60] but for the time being, without greater resolution, we cannot make definitive assignments but merely speculate that among the multitudes of absorption lines observed around 9063 and 8958 Å, some might belong to C_{60}^+.

V. CONCLUSIONS

Here, we have reviewed and revised the data from a previous photoionization study of the C_{60} Buckminsterfullerene.[19] By re-treating this original dataset, we have obtained a TPES that exhibits several sharp resonances that are assigned to the ground state of C_{60}^+. In the previous treatment, these sharp resonances were lost, which required an interpretation of the results in terms of previous gas phase measurements that appeared to evidence D_{3d} symmetry of the cationic ground state. This revised interpretation compares exceptionally well with the previously computed photoelectron spectrum presented in the work of Manini *et al.*[18] based on a vibronic model and underlines that the ground state symmetry of gas phase C_{60}^+ is D_{5d} symmetric. This reconciliates PES-based (along with IR- and optical-based) conclusions about the ground state symmetry of C_{60}^+ in frozen noble gas matrices and gas phase measurements.[8,21,40] This in turn allows us to assign the first adiabatic ionization transition and thus determine the ionization energy of C_{60} with greater accuracy than has been achieved at 7.598 ± 0.005 eV, tentatively assign the onsets of the $^2E_{1u}$ and $^2E_{2u}$ excited states around 7.865 ± 0.005, and 7.882 ± 0.005 eV, respectively, and postulate on the energetics of additional DIBs that may be assigned to C_{60}^+ in the future.

In complement with the comparison of the experimental TPES with the vibronic spectrum presented in the work of Manini *et al.*, we have also investigated the effects of temperatures on IR spectra and PES and discussed the magnitude of anharmonicities via DFTB and TD-DFTB calculations coupled with classical MD. Good agreement is found with literature concerning the IR spectra of both C_{60} and C_{60}^+, and the simulations at various temperatures inform on the possible magnitude of anharmonic effects. The magnitude of the anharmonicities obtained for C_{60} agrees with the theoretical and experimental data of other authors and appear too weak to explain the blue shifts of the peaks in the vibronic model with respect to experimental TPES. Simulations of IR spectra of C_{60}^+ show that temperature effects are larger, whereas they cannot receive simple linear extrapolation due to the presence of the Jahn–Teller conical intersection. Finally, classical MD simulations of the PES with DFTB reasonably reproduce the overall envelopes of the experimental features considering a D_{5d} symmetry in the ground state of C_{60}^+ (without vibrational resolution), also analyzing its evolution with temperature.

SUPPLEMENTARY MATERIAL

The supplementary material includes mass-selected ion images and their projections along the direction of the molecular beam and close-ups of the re-treated TPES used to investigate anharmonic shifts and comparisons with recent vibrational and electronic spectra of C_{60}^+.

ACKNOWLEDGMENTS

We are grateful to SOLEIL for provision of synchrotron radiation under Proposal No. 20180297, as well as to J.-F. Gil for his technical assistance on the SAPHIRS endstation. H.R.H. is grateful for support from the Marie Sklodowska Curie actions, Proposal No. 838372. The authors also acknowledge the HPC mesocenter CALMIP (UMS CNRS 3667) for the allocation of computer resources (Grant Nos. p0059 and p18009). The authors would like to acknowledge and appreciate the contribution of the late Professor Harold Linnartz, who suddenly and mournfully passed away during the final stages of the preparation of this manuscript. Our heartfelt condolences go to his family and loved ones.

AUTHOR DECLARATIONS

Conflict of Interest

The authors have no conflicts to disclose.

Author Contributions

Helgi Rafn Hrodmarsson: Conceptualization (lead); Data curation (lead); Formal analysis (equal); Investigation (equal); Methodology (equal); Project administration (supporting); Resources (supporting); Validation (equal); Visualization (equal); Writing – original draft (lead); Writing – review & editing (lead). **Mathias Rapacioli**: Data curation (equal); Formal analysis (equal); Investigation (equal); Methodology (equal); Validation (equal); Visualization (equal); Writing – review & editing (equal). **Fernand Spiegelman**: Data curation (equal); Formal analysis (equal); Investigation (equal); Methodology (equal); Validation (equal); Visualization (equal); Writing – review & editing (equal). **Gustavo A. Garcia**: Formal analysis (equal); Investigation (equal); Methodology (equal); Validation (equal); Visualization (equal); Writing – review & editing (equal). **Jordy Bouwman**: Formal analysis (equal); Investigation (equal); Validation (equal); Visualization (equal); Writing – review & editing (equal). **Laurent Nahon**: Formal analysis (equal); Investigation (equal); Project administration (equal); Resources (equal); Supervision (equal); Validation (equal); Writing – review & editing (equal). **Harold Linnartz**: Funding acquisition (equal); Project administration (equal); Resources (equal); Supervision (equal); Writing – review & editing (equal).

DATA AVAILABILITY

The data that support the findings of this study are available from the corresponding author upon reasonable request.

REFERENCES

[1] M. L. Heger, "Further study of the sodium lines in class B stars," Lick Obs. Bull. **10**, 141–145 (1922).
[2] B. A. McGuire, "2021 census of interstellar, circumstellar, extragalactic, protoplanetary disk, and exoplanetary molecules," Astrophys. J., Suppl. Ser. **259**, 51 (2022).
[3] E. K. Campbell, M. Holz, D. Gerlich, and J. P. Maier, "Laboratory confirmation of C_{60}^+ as the carrier of two diffuse interstellar bands," Nature **523**(7560), 322 (2015).

[4]M. A. Cordiner, H. Linnartz, N. L. J. Cox, J. Cami, F. Najarro, C. R. Proffitt, R. Lallement, P. Ehrenfreund, B. H. Foing, T. R. Gull, P. J. Sarre, and S. B. Charnley, "Confirming interstellar C_{60}^+ using the hubble space telescope," Astrophys. J. Lett. **875**(2), L28 (2019).
[5]H. Linnartz, J. Cami, M. Cordiner, N. L. J. Cox, P. Ehrenfreund, B. Foing, M. Gatchell, and P. Scheier, "C_{60}^+ as a diffuse interstellar band carrier; a spectroscopic story in 6 acts," J. Mol. Spectrosc. **367**, 111243 (2020).
[6]G.-L. Hou, O. V. Lushchikova, J. M. Bakker, P. Lievens, L. Decin, and E. Janssens, "Buckyball-metal complexes as potential carriers of astronomical unidentified infrared emission bands," Astrophys. J. **952**(1), 13 (2023).
[7]O. Berné, G. Mulas, and C. Joblin, "Interstellar C_{60}^+," Astron. Astrophys. **550**, L4 (2013).
[8]B. Kern, D. Strelnikov, P. Weis, A. Böttcher, and M. M. Kappes, "IR absorptions of C_{60}^+ and C_{60}^- in neon matrixes," J. Phys. Chem. A **117**(34), 8251–8255 (2013).
[9]A. Ceulemans and P. Fowler, "The Jahn–Teller instability of fivefold degenerate states in icosahedral molecules," J. Chem. Phys. **93**(2), 1221–1234 (1990).
[10]H. Ramanantoanina, J. T. Muya, A. Ceulemans, and C. Daul, "C_{60}^+ and B_{80}^+: A comparative study of the Jahn-Teller effect," J. Phys.: Conf. Ser. **428**, 012005 (2013).
[11]Z. Huang and D. Liu, "First principles study of the vibronic coupling in positively charged C_{60}^+," Chem. Phys. Lett. **754**, 137698 (2020).
[12]C. Moate, J. Dunn, C. Bates, and Y. Liu, "An analytical model for the $H \otimes (h \oplus g)$ Jahn-Teller system," J. Phys.: Condens.Matter **9**(28), 6049–6060 (1997).
[13]I. D. Hands, L. M. Sindi, J. L. Dunn, and C. A. Bates, "Theoretical treatment of pseudorotation in the Jahn-Teller C_{60}^+ ion," Phys. Rev. B **74**(11), 115410 (2006).
[14]A. O. Lykhin, S. Ahmadvand, and S. A. Varganov, "Electronic transitions responsible for C_{60}^+ diffuse interstellar bands," J. Phys. Chem. Lett. **10**(1), 115–120 (2019).
[15]S. Canton, A. Yencha, E. Kukk, J. Bozek, M. Lopes, G. Snell, and N. Berrah, "Comment on 'Experimental evidence of a dynamic Jahn-Teller effect in C_{60}^+' - Reply," Phys. Rev. Lett. **90**(24), 249602 (2003).
[16]N. Manini and E. Tosatti, "Comment on 'Experimental evidence of a dynamic Jahn-Teller effect in C_{60}^+,'" Phys. Rev. Lett. **90**(24), 249601 (2003).
[17]S. Canton, A. Yencha, E. Kukk, J. Bozek, M. Lopes, G. Snell, and N. Berrah, "Experimental evidence of a dynamic Jahn-Teller effect in C_{60}^+," Phys. Rev. Lett. **89**(4), 045502 (2002).
[18]N. Manini, P. Gattari, and E. Tosatti, "Jahn-Teller spectral fingerprint in molecular photoemission: C_{60}," Phys. Rev. Lett. **91**(19), 196402 (2003).
[19]H. R. Hrodmarsson, G. A. Garcia, H. Linnartz, and L. Nahon, "VUV photoionization dynamics of the C_{60} buckminsterfullerene: 2D-matrix photoelectron spectroscopy in an astrophysical context," Phys. Chem. Chem. Phys. **22**, 13880–13892 (2020).
[20]N. Manini, A. Dal Corso, M. Fabrizio, and E. Tosatti, "Electron-vibration coupling constants in positively charged fullerene," Philos. Mag. B **81**(8), 793–812 (2001).
[21]M. Kappe, A. Schiller, E. Gruber, D. Jank, M. Gatt, G. Schöpfer, M. Oncak, A. M. Ellis, and P. Scheier, "Spectroscopy of C_{60}^+ and C_{120}^+ in the mid-infrared," J. Chem. Phys. **159**(20), 204302 (2023).
[22]I. Hertel, H. Steger, J. de Vries, B. Weisser, C. Menzel, B. Kamke, and W. Kamke, "Giant plasmon excitation in free C_{60} and C_{70} molecules studied by photoionization," Phys. Rev. Lett. **68**(6), 784–787 (1992).
[23]J. de Vries, H. Steger, B. Kamke, C. Menzel, B. Weisser, W. Kamke, and I. Hertel, "Single-photon ionization of C_{60} fullerene and C_{70} fullerene with synchrotron radiation: Determination of the ionization-potential of C_{60}," Chem. Phys. Lett. **188**(3–4), 159–162 (1992).
[24]R. Yoo, B. Ruscic, and J. Berkowitz, "Vacuum ultraviolet photoionization mass-spectrometric study of C_{60}," J. Chem. Phys. **96**(2), 911–918 (1992).
[25]L. Nahon, N. de Oliveira, G. A. Garcia, J.-F. Gil, B. Pilette, O. Marcouille, B. Lagarde, and F. Polack, "DESIRS: A state-of-the-art VUV beamline featuring high resolution and variable polarization for spectroscopy and dichroism at SOLEIL," J. Synchrotron Radiat. **19**(4), 508–520 (2012).
[26]G. A. Garcia, B. K. C. de Miranda, M. Tia, S. Daly, and L. Nahon, "DELICIOUS III: A multipurpose double imaging particle coincidence spectrometer for gas phase vacuum ultraviolet photodynamics studies," Rev. Sci. Instrum. **84**(5), 053112 (2013).
[27]X. Tang, G. A. Garcia, J.-F. Gil, and L. Nahon, "Vacuum upgrade and enhanced performances of the double imaging electron/ion coincidence end-station at the vacuum ultraviolet beamline DESIRS," Rev. Sci. Instrum. **86**(12), 123108 (2015).
[28]G. Garcia, L. Nahon, and I. Powis, "Two-dimensional charged particle image inversion using a polar basis function expansion," Rev. Sci. Instrum. **75**(11), 4989–4996 (2004).
[29]J. C. Poully, J. P. Schermann, N. Nieuwjaer, F. Lecomte, G. Gregoire, C. Desfrancois, G. A. Garcia, L. Nahon, D. Nandi, L. Poisson, and M. Hochlaf, "Photoionization of 2-pyridone and 2-hydroxypyridine," Phys. Chem. Chem. Phys. **12**(14), 3566–3572 (2010).
[30]F. Spiegelman, N. Tarrat, J. Cuny, L. Dontot, E. Posenitskiy, C. Martí, A. Simon, and M. Rapacioli, "Density-functional tight-binding: Basic concepts and applications to molecules and clusters," Adv. Phys.: X **5**(1), 1710252 (2020).
[31]M. Elstner and G. Seifert, "Density functional tight binding," Philos. Trans. R. Soc., A **372**(2011), 20120483 (2014).
[32]M. Rapacioli, T. Heine, L. Dontot, M. Yusef Buey, E. Posenitskiy, N. Tarrat, F. Spiegelman, C. Louisnard, C. Marti, J. Cuny, M. Morniere, C. Dubosq, J. Frenzel, E. Michoulier, H. Duarte, L. Zchekhov, and D. Salahub, deMonNano Software, http://www.demon-software.com.
[33]J. Frenzel, A. F. Oliveira, N. Jardillier, T. Heine, and G. Seifert, "Semi-relativistic, self-consistent charge Slater-Koster tables for density-functional based tight-binding (DFTB) for materials science simulations," TU-Dresden 2004-2009; available at https://dftb.org/parameters/download/matsci/matsci-0-3-cc.
[34]S. Chakraborty, G. Mulas, M. Rapacioli, and C. Joblin, "Anharmonic infrared spectra of thermally excited pyrene ($C_{16}H_{10}$): A combined view of DFT-based GVPT2 with AnharmonicCaOs, and approximate DFT molecular dynamics with demonNano," J. Mol. Spectrosc. **378**, 111466 (2021).
[35]Y. Sugita and Y. Okamoto, "Replica-exchange molecular dynamics method for protein folding," Chem. Phys. Lett. **314**(1–2), 141–151 (1999).
[36]L. F. L. Oliveira, J. Cuny, M. Morinière, L. Dontot, A. Simon, F. Spiegelman, and M. Rapacioli, "Phase changes of the water hexamer and octamer in the gas phase and adsorbed on polycyclic aromatic hydrocarbons," Phys. Chem. Chem. Phys. **17**(26), 17079–17089 (2015).
[37]T. A. Niehaus, "Approximate time-dependent density functional theory," J. Mol. Struct.: THEOCHEM **914**(1–3), 38–49 (2009).
[38]C. Dubosq, F. Calvo, M. Rapacioli, E. Dartois, T. Pino, C. Falvo, and A. Simon, "Quantum modeling of the optical spectra of carbon cluster structural families and relation to the interstellar extinction UV bump," Astron. Astrophys. **634**, A62 (2020).
[39]N. Manini and P. De Los Rios, "Berry phase and ground state symmetry in $H \otimes h$ dynamical Jahn-Teller systems," Phys. Rev. B **62**(1), 29–32 (2000).
[40]D. Gerlich, J. Jasik, D. V. Strelnikov, and J. Roithova, "IR spectroscopy of fullerene ions in a cryogenic quadrupole trap," Astrophys. J. **864**(1), 62 (2018).
[41]H. Yasumatsu, T. Kondow, H. Kitagawa, K. Tabayashi, and K. Shobatake, "Absorption spectrum of C_{60} in the gas phase: Autoionization via core-excited Rydberg states," J. Chem. Phys. **104**(3), 899–902 (1996).
[42]P. Kupser, J. D. Steill, J. Oomens, G. Meijer, and G. von Helden, "IR spectroscopy of gas-phase C_{60}^-," Phys. Chem. Chem. Phys. **10**(45), 6862 (2008).
[43]L. Nemes, R. S. Ram, P. F. Bernath, F. A. Tinker, M. C. Zumwalt, L. D. Lamb, and D. R. Huffman, "Gas-phase infrared emission spectra of C_{60} and C_{70}. Temperature-dependent studies," Chem. Phys. Lett. **218**(4), 295–303 (1994).
[44]R. C. Haddon, L. E. Brus, and K. Raghavachari, "Electronic structure and bonding in icosahedral C_{60}," Chem. Phys. Lett. **125**(5–6), 459–464 (1986).
[45]D. S. Bethune, G. Meijer, W. C. Tang, H. J. Rosen, W. G. Golden, H. Seki, C. A. Brown, and M. S. de Vries, "Vibrational Raman and infrared spectra of chromatographically separated C_{60} and C_{70} fullerene clusters," Chem. Phys. Lett. **179**(1–2), 181–186 (1991).
[46]K. Raghavachari and C. M. Rohlfing, "Structures and vibrational frequencies of carbon molecules (C_{60}, C_{70}, and C_{84})," J. Phys. Chem. **95**(15), 5768–5773 (1991).
[47]C. Z. Wang, C. T. Chan, and K. M. Ho, "Structure and dynamics of C_{60} and C_{70} from tight-binding molecular dynamics," Phys. Rev. B **46**(15), 9761–9767 (1992).

[48]F. Negri, G. Orlandi, and F. Zerbetto, "Quantum-chemical investigation of Franck-Condon and Jahn-Teller activity in the electronic spectra of Buckminsterfullerene," Chem. Phys. Lett. **144**(1), 31–37 (1988).
[49]F. Negri, G. Orlandi, and F. Zerbetto, "QCFF/PI vibrational frequencies of some spherical carbon clusters," J. Am. Chem. Soc. **113**(16), 6037–6040 (1991).
[50]A. Bekkerman, E. Kolodney, G. von Helden, B. Sartakov, D. van Heijnsbergen, and G. Meijer, "Infrared multiphoton ionization of superhot C_{60}: Experiment and model calculations," J. Chem. Phys. **124**(18), 184312 (2006).
[51]H. Wang and M. S. Daw, "Anharmonicity of vibrational modes in fullerenes," Comput. Mater. Sci. **146**, 70–72 (2018).
[52]A. V. Talyzin, A. Dzwilewski, and T. Wagberg, "Temperature dependence of C_{60} Raman spectra up to 840 K," Solid State Commun. **140**(3–4), 178–181 (2006).
[53]F. Cataldo, S. Iglesias-Groth, and A. Manchado, "Low and high temperature infrared spectroscopy of C_{60} and C_{70} fullerenes," Fullerenes, Nanotubes Carbon Nanostruct. **18**(3), 224–235 (2010).
[54]D. Strelnikov, B. Kern, and M. M. Kappes, "On observing C_{60}^{+} and C_{60}^{2+} in laboratory and space," Astron. Astrophys. **584**, A55 (2015).
[55]P. A. Brühwiler, A. J. Maxwell, P. Baltzer, S. Andersson, D. Arvanitis, L. Karlsson, and N. Mårtensson, "Vibronic coupling in the photoemission bands of condensed C_{60}," Chem. Phys. Lett. **279**(1–2), 85–91 (1997).
[56]E. K. Campbell, M. Holz, J. P. Maier, D. Gerlich, G. A. H. Walker, and D. Bohlender, "Gas phase absorption spectroscopy of C_{60}^{+} and C_{70}^{+} in a cryogenic ion trap: Comparison with astronomical measurements," Astrophys. J. **822**(1), 17 (2016).
[57]E. K. Campbell, M. Holz, and J. P. Maier, "C_{60}^{+} in diffuse clouds: Laboratory and astronomical comparison," Astrophys. J. Lett. **826**(1), L4 (2016).
[58]M. Kuhn, M. Renzler, J. Postler, S. Ralser, S. Spieler, M. Simpson, H. Linnartz, A. G. G. M. Tielens, J. Cami, A. Mauracher, Y. Wang, M. Alcami, F. Martin, M. K. Beyer, R. Wester, A. Lindinger, and P. Scheier, "Atomically resolved phase transition of fullerene cations solvated in helium droplets," Nat. Commun. **7**, 13550 (2016).
[59]G. von Helden, I. Holleman, G. M. H. Knippels, A. F. G. van der Meer, and G. Meijer, "Infrared resonance enhanced multiphoton ionization of fullerenes," Phys. Rev. Lett. **79**(26), 5234–5237 (1997).
[60]N. L. J. Cox, J. Cami, A. Farhang, J. Smoker, A. Monreal-Ibero, R. Lallement, P. J. Sarre, C. C. M. Marshall, K. T. Smith, C. J. Evans, P. Royer, H. Linnartz, M. A. Cordiner, C. Joblin, J. Th. van Loon, B. H. Foing, N. H. Bhatt, E. Bron, M. Elyajouri, A. de Koter, P. Ehrenfreund, A. Javadi, L. Kaper, H. G. Khosroshadi, M. Laverick, F. Le Petit, G. Mulas, E. Roueff, F. Salama, and M. Spaans, "The ESO diffuse interstellar bands large exploration survey (EDIBLES): I. Project description, survey sample, and quality assessment," Astron. Astrophys. **606**, A76 (2017).